Magnetic Resonance in Medicine 72:389–398 (2014)

Strategies for Improved 3D Small-Tip Fast Recovery Imaging

Hao Sun,[1]* Jeffrey A. Fessler,[1,2] Douglas C. Noll,[2] and Jon-Fredrik Nielsen[2]

Purpose: Small-tip fast recovery (STFR) imaging is a recently proposed steady-state sequence that has similar image contrast as balanced steady-state free precession but has the potential to simultaneously remove banding artifacts and transient fluctuation. STFR relies on a "tip-up" radiofrequency (RF) pulse tailored to the accumulated phase during the free precession (data acquisition) interval, designed to bring spins back to the longitudinal axis, thereby preserving transverse magnetization as longitudinal magnetization for the next pulse repetition time. We recently proposed an RF-spoiled STFR sequence suitable for thin slab imaging, however, in many applications, e.g., functional magnetic resonance imaging or isotropic-resolution structural imaging, three-dimensional (3D) steady-state imaging is desirable. Unfortunately, 3D STFR imaging is challenging due to the need for 3D tailored RF pulses. Here, we propose new strategies for improved 3D STFR imaging, based on (i) unspoiled imaging, and (ii) joint design of nonslice-selective tip-down/tip-up RF pulses.

Theory and Methods: We derive an analytic signal model for the proposed unspoiled STFR sequence, and propose two strategies for designing the 3D tailored tip-down/tip-up RF pulses. We validate the analytic results using phantom and in vivo imaging experiments.

Results: Our analytic model and imaging experiments demonstrate that the proposed unspoiled STFR sequence is less sensitive to tip-up excitation error compared to the corresponding spoiled sequence, and may, therefore, be an attractive candidate for 3D imaging. The proposed "joint" RF pulse design method, in which we formulate the tip-down/tip-up RF pulse design task as a magnitude least squares problem, produces modest improvement over a simpler "Separate" design approach. Using the proposed unspoiled sequence and joint RF pulse design, we demonstrate proof-of-principle 3D STFR brain images with balanced steady-state free precession-like signal properties but with reduced banding.

Conclusion: Using the proposed unspoiled sequence and joint RF pulse design, STFR brain images in a 3D region of interest with balanced steady-state free precession-like signal properties but with reduced banding can be obtained. **Magn Reson Med 72:389–398, 2014. © 2013 Wiley Periodicals, Inc.**

Key words: steady-state magnetic resonance imaging; pulse design; balanced steady-state free precession; banding artifact; small-tip fast recovery

INTRODUCTION

Balanced steady-state free precession (bSSFP) is a rapid imaging sequence that has high signal-to-noise ratio (SNR) and useful tissue contrast, but suffers from off-resonance banding artifacts and transient fluctuations (1). Numerous methods have been proposed in the past decade for correcting these artifacts, including multi-pulse repetition time (TR) sequences that seek to widen the separation between bands (2–5), and multiple phase-cycled acquisitions that are combined to produce uniform signal independent of off-resonance. However, all of these methods sacrifice signal strength and/or imaging time, and are not universally applicable to all bSSFP applications.

Recently, our group proposed a new steady state imaging sequence called small-tip fast recovery (STFR) (6), which is a potential alternative to bSSFP. There are two key ideas in STFR: First, after excitation and readout, a tip-up radiofrequency (RF) pulse tailored to the accumulated phase during free precession is transmitted to bring spins back to the longitudinal-axis, which "fast recovers" the transverse magnetization and preserves it as longitudinal magnetization for the next TR (6,7). Second, after the tip-up pulse, it is necessary to play an unbalanced gradient to dephase residual transverse spins. With accurate tailored pulses, STFR imaging may have many of the benefits of bSSFP such as high SNR efficiency, good flow properties, and combined T2/T1 weighting (1), but does not suffer from banding artifacts. STFR, therefore, has the potential to provide an alternative to bSSFP for some applications, and may obviate the need for special artifact-reduction techniques such as phase-cycled imaging (8) or multiple-TR sequences (2–5).

However, STFR is challenging to implement in practice, due to the need for accurate tailored tip-up pulses. This is particularly true in three-dimensional (3D) imaging, as the required 3D tailored pulses can be prohibitively long. Here, we propose new strategies for improved 3D STFR imaging, based on (i) unspoiled imaging, and (ii) joint design of nonslice-selective tip-down/tip-up 3D tailored RF pulses.

We begin this article by deriving an analytic signal equation for the proposed unspoiled STFR sequence, which is then used to compare the properties of

[1]Department of Electrical Engineering and Computer Science, University of Michigan, Ann Arbor, Michigan, USA.

[2]Department of Biomedical Engineering, University of Michigan, Ann Arbor, Michigan, USA.

Grant sponsor: NIH; Grant number: R21EB012674; Grant sponsor: NIH; Grant number: R01NS58576.

*Correspondence to: Hao Sun, M.S., 1073 B.I.R.B., 2360 Bonisteel Ave., Ann Arbor, MI 48109-2108, E-mail: sunhao@umich.edu

Received 3 April 2013; revised 15 August 2013; accepted 19 August 2013

DOI 10.1002/mrm.24947

Published online 11 October 2013 in Wiley Online Library (wileyonlinelibrary.com).

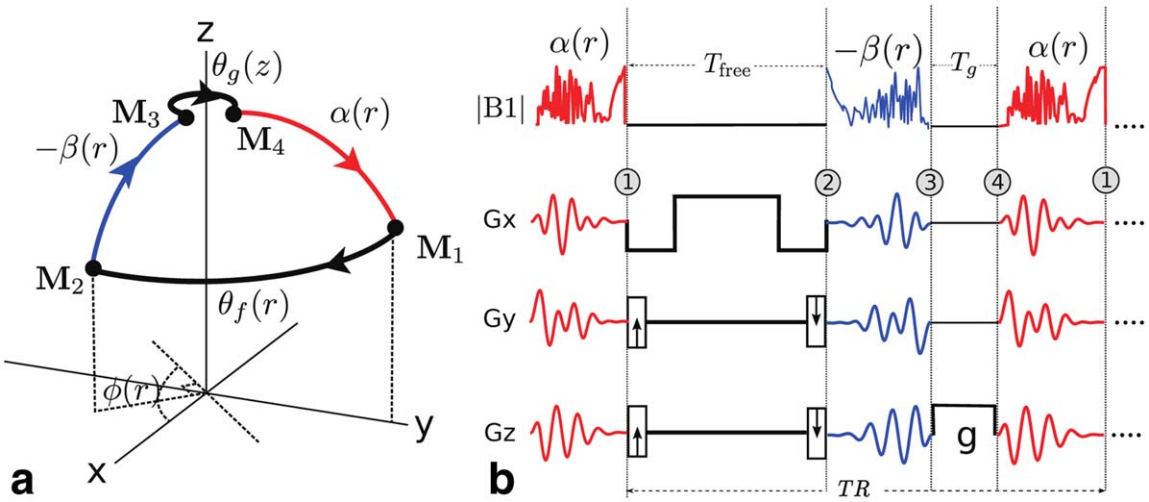

FIG. 1. Proposed "unspoiled STFR" pulse sequence. **a**: Steady-state path for a spin isochromat. The spin is tipped back to the longitudinal axis by a tailored pulse with flip angle $-\beta(\mathbf{r})$ and phase $\phi(\mathbf{r}).\phi(\mathbf{r})$ is designed to be equal to the accumulated free precession angle $\theta_f(\mathbf{r}) = \Delta\omega(\mathbf{r})T_{\text{free}}$, where T_{free} is the free precession time. **b**: Example pulse sequence diagram, using tailored pulses for both tip-down (red) and tip-up (blue) excitations, and 3D Cartesian data readout. [Color figure can be viewed in the online issue, which is available at wileyonlinelibrary.com.]

unspoiled and spoiled STFR. We then describe the proposed Joint RF pulse design algorithm that treats the tip-down and tip-up pulses as one combined RF pulse, which is in turn designed using magnitude least-squares optimization. Next, we describe our experimental methods and results (phantom and in vivo), demonstrating that the proposed unspoiled STFR sequence is less sensitive to tip-up excitation error compared to the spoiled sequence in (6) and hence is a promising candidate for 3D imaging. We conclude with a discussion of limitations and future extensions of this work.

THEORY

Unspoiled STFR

The proposed unspoiled STFR sequence and associated spin path are illustrated in Figure 1a. The spin is first tipped down by a small tip angle pulse with flip angle $\alpha(\mathbf{r})$. This tip-down pulse can be spatially tailored, i.e., the flip angle (magnitude and phase) may vary with the spatial coordinate $\mathbf{r}$. During the signal readout interval T_{free}, the spin precesses by an angle $\theta_f(\mathbf{r}) = \Delta\omega(\mathbf{r})T_{\text{free}}$, where $\Delta\omega(\mathbf{r})$ is the off-resonance frequency ($B0$ inhomogeneity) at position $\mathbf{r}$. A "tip-up," or "fast recovery," RF pulse with flip angle $\beta(\mathbf{r})$ tailored to the accumulated phase $\theta_f(\mathbf{r})$ is then transmitted to bring the magnetization vector back toward the longitudinal axis. The purpose of the tip-up pulse is to preserve as much longitudinal magnetization as possible prior to the next sequence repetition interval (TR) and hence to maximize SNR efficiency, and to introduce T_2 weighting. Immediately after the tip-up pulse, an unbalanced gradient g is played out, designed to dephase the residual transverse magnetization left over after the tip-up pulse. This gradient causes a rotation θ_g of each spin isochromat, with θ_g varying along the direction of g. We will see below that this unbalanced gradient is necessary for banding-free imaging. Note that the RF phase offset from TR-to-TR is held constant, i.e., we do not use RF-spoiling [quadratic phase cycling, as was done in (6)] in the sequence proposed here.

Steady-state Magnetization for a Spin Isochromat

To obtain a signal equation for unspoiled STFR, we first develop an expression for the steady state magnetization $\mathbf{M}_1(\theta_g)$ for a spin isochromat immediately after the tip-down pulse (see Figure 1a), and then integrate the resulting expression over all isochromats within a voxel, i.e., we integrate over $\theta_g = [0, 2\pi]$. For clarity, we drop the explicit dependence on spatial position $\mathbf{r}$ in the following.

Without loss of generality, our derivation assumes the tip-down pulse to be aligned with the x-axis (zero phase). We ignore the RF pulse duration (which can vary depending on, e.g., excitation k-space trajectory), which is a common assumption when deriving analytic models for steady-state sequences, especially for RF pulses that are short compared to TR (9). We obtain the steady-state magnetization by modeling each step of the spin path using the Bloch equation in matrix form. Details of the derivation are provided in the Appendix. We obtain the following expression for the steady-state transverse magnetization of a spin isochromat:

$$M_{1,t} = M_0 \frac{a\cos(\theta_g + \phi) + b\sin(\theta_g + \phi) + c}{d\cos(\theta_g + \phi) + e\sin(\theta_g + \phi) + f} \qquad [1]$$

where $M_{1,t}$ is the transverse component of M_1, M_0 is the equilibrium magnetization and the factors a through f are defined as:

$$a = -iE_{g2}(E_{f2}(-1 + E_{g1} + (-1 + E_{f1})E_{g1}\cos\beta)\cos(\theta_f - \phi)\sin\alpha + (E_{f1}(-1 + E_{g1}) + (-1 + E_{f1})\cos\alpha)\sin\beta + iE_{f2}(-1 + E_{g1} + (-1 + E_{f1})E_{g1}\cos\beta)\sin\alpha\sin(\theta_f - \phi))$$

$$b = E_{g2}(E_{f2}((-1 + E_{f1})E_{g1} + (-1 + E_{g1})\cos\beta)\cos(\theta_f - \phi)\sin\alpha - (-1 + E_{f1} + E_{f1}(-1 + E_{g1})\cos\alpha)\sin\beta + iE_{f2}((-1 + E_{f1})E_{g1} + (-1 + E_{g1})\cos\beta)\sin\alpha\sin(\theta_f - \phi))$$

$$c = i((-1 + E_{g1} + (-1 + E_{f1})E_{g1}\cos\beta)\sin\alpha + E_{f2}E_{g2}^2(E_{f1}(-1 + E_{g1}) + (-1 + E_{f1})\cos\alpha)\sin\beta(\cos(\theta_f - \phi) + i\sin(\theta_f - \phi)))$$

$$d = E_{g2}(-E_{f2}(-1 + E_{f1}E_{g1})(1 + \cos\alpha\cos\beta)\cos(\theta_f - \phi) + (E_{f1} - E_{f2}^2E_{g1})\sin\alpha\sin\beta)$$

$$e = E_{f2}(-1 + E_{f1}E_{g1})E_{g2}(\cos\alpha + \cos\beta)\sin(\theta_f - \phi)$$

$$f = -1 + E_{f1}E_{f2}^2E_{g1}E_{g2}^2 + (E_{f1}E_{g1} - E_{f2}^2E_{g2}^2)\cos\alpha\cos\beta + E_{f2}(E_{g1} - E_{f1}E_{g2}^2)\cos(\theta_f - \phi)\sin\alpha\sin\beta$$

In the above expression, the T_1 and T_2 relaxation exponentials during the free precession and gradient dephasing intervals are denoted as $E_{f1} = e^{-T_{\text{free}}/T_1}$, $E_{f2} = e^{-T_{\text{free}}/T_2}$, $E_{g1} = e^{-T_g/T_1}$, and $E_{g2} = e^{-T_g/T_2}$.

Although Eq. [1] is only an intermediate expression needed to obtain the total voxel signal, it is instructive to examine its dependence on θ_g when the tip-up pulse is perfectly matched to the spin precession angle, i.e., $\phi = \theta_f$ and $\beta = \alpha$. Then, the θ_f terms in the coefficients *a* through *f* are canceled by ϕ, and these coefficients, therefore, become independent of the local off-resonance. $M_{1,t}$ then depends on off-resonance only through $\cos(\phi + \theta_g)$ and $\sin(\phi + \theta_g)$. Figure 2 plots Eq. [1] under these conditions, for $T_1/T_2 = 510/50$ ms and $\alpha = \beta = 16°$. The most striking feature of Figure 2 is the presence of narrow minima spaced 2π apart, which explains why fully balanced ($g = 0$ and thus $\theta_g = 0$) STFR imaging would be problematic, as narrow bands would be present in regions of the image where ϕ (and θ_f) equals an integer multiple of 2π. The minima in Figure 2 are reminiscent of dark signal bands in bSSFP, except for one crucial difference: the neighboring "bands" in Figure 2 are in-phase. We, therefore, expect the total voxel signal for unbalanced STFR, obtained by integrating over one full cycle (shaded region) in Figure 2, to be high and contain no such banding artifacts.

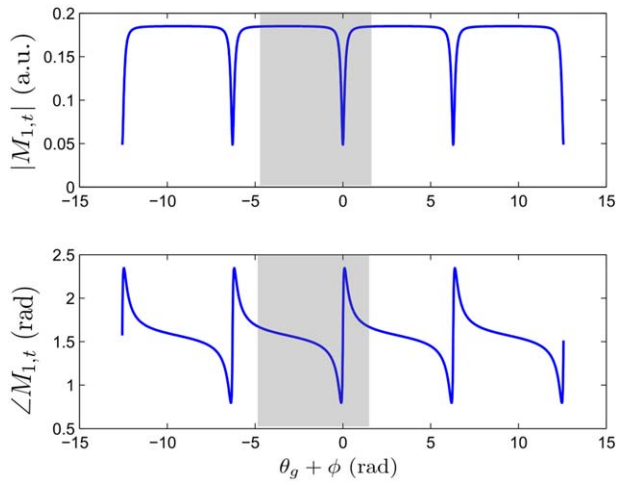

FIG. 2. Steady-state magnetization (Eq. [1]) for a spin isochromat as a function of $\phi + \theta_g$, where ϕ is the phase of the tip-up pulse and θ_g is the precession induced by the applied unbalanced gradient. Narrow bands are spaced 2π apart, and neighboring bands are equal both in magnitude and phase. In the proposed unbalanced STFR sequence, the signal from a voxel can be calculated by integrating over one full cycle (shaded region). The result of this integration is given by Eq. [2]. [Color figure can be viewed in the online issue, which is available at wileyonlinelibrary.com.]

Signal Equation

To obtain the steady-state signal M_t from a voxel, we integrate $M_{1,t}(\theta_g)$ over the full distribution of spins:

$$\begin{aligned} M_t(\phi, \theta_f, \alpha, \beta, T_1, T_2, T_{\text{free}}, T_g) &= \frac{1}{2\pi}\int_0^{2\pi} M_{1,t}(\phi + \theta_g)d\theta_g \\ &= M_0\frac{1}{2\pi}\int_0^{2\pi}\frac{a\cos(\theta_g + \phi) + b\sin(\theta_g + \phi) + c}{d\cos(\theta_g + \phi) + e\sin(\theta_g + \phi) + f}d\theta_g \\ &= M_0\left(\frac{c}{\sqrt{f^2 - d^2 - e^2}} - \frac{ad + be}{d^2 + e^2}\frac{f - \sqrt{f^2 - d^2 - e^2}}{\sqrt{f^2 - d^2 - e^2}}\right) \end{aligned} \quad [2]$$

Here, we denote the dependence on the various tissue and sequence parameters on the left-hand side only. Equation [2] describes the signal from a voxel immediately after the tip-down pulse, and must be multiplied by $e^{-\text{TE}/T_2 - i\text{TE}\Delta\omega}$ to obtain the signal at the echo time. Equation [2] is valuable in several respects: First, it provides a fast way to analyze the sequence properties and optimize the imaging parameters. Second, it shows that the STFR signal is independent of off-resonance if we have a perfectly tailored pulse (off-resonance induced phase θ_f is canceled out by ϕ in coefficients *a* through *f*). Finally, this expression can be used to describe the extended Chimera sequence (10) that is similar to our unspoiled STFR except conventional RF pulses are used instead of tailored pulses.

Figure 3a plots Eq. [2] over a range of flip angles, for three different tissue types. Here, we assume that the tip-up pulse is ideal, i.e., $\phi = \theta_f$ and $\beta = \alpha$. For comparison, the calculated signals for bSSFP and spoiled STFR are also shown, using analytic results from (11) and (6),

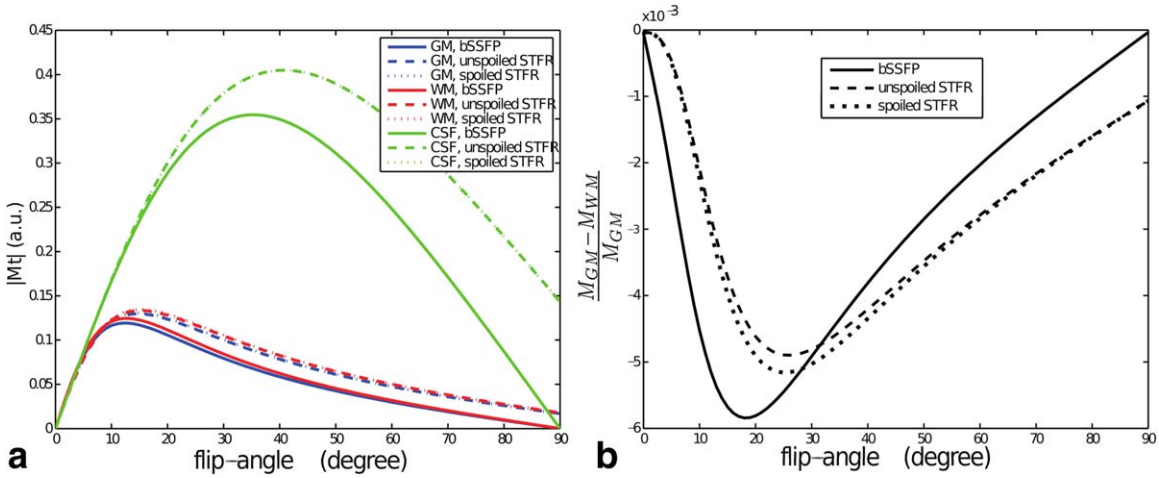

FIG. 3. Predicted tissue signal for unspoiled STFR (Eq. [2]), spoiled STFR (6) and bSSFP (11). These calculations assumed $T_1/T_2 = 4000/2000$, 1470/71, and 1110/56 ms for CSF, gray matter, and white matter, respectively (12). The bSSFP curves were calculated using a flip angle of 2α, which is expected to produce similar signal contrast as STFR using a flip angle of α. **a**: STFR produces similar signal as bSSFP, as desired. **b**: STFR and bSSFP are predicted to have similar gray/white matter contrast. [Color figure can be viewed in the online issue, which is available at wileyonlinelibrary.com.]

respectively. Notice, we use twice the flip angle of STFR sequences in the calculation of bSSFP signals. Figure 3b plots the corresponding white/gray matter contrast. We see that unspoiled STFR produces similar tissue signal and contrast as bSSFP, as desired.

Figure 4a plots Eq. [2] as a function of the phase mismatch $\phi - \theta_f$ between the tip-up phase ϕ and the spin phase θ_f. Such a phase mismatch is unavoidable in practice, as the tip-up pulse will never be perfectly accurate everywhere within the imaging region of interest (ROI). For comparison, the corresponding plot for spoiled STFR is also shown. In addition, experimentally observed signal curves are plotted, obtained by applying a linear gradient shim and imaging with sinc (i.e., untailored) tip-down and tip-up pulses (see Figure 4b). The analytic curve was calculated based on the actual T_1, T_2 values of the phantom ($T_1/T_2 = 510/50$ ms), which were measured using inversion recovery and spin echo sequences, respectively. The signal for both unspoiled and spoiled STFR depends on $\phi - \theta_f$, but unspoiled STFR decays less rapidly with increasing phase error. In other words, unspoiled STFR is less sensitive to tip-up phase error compared to spoiled STFR. The difference in the rate of signal drop versus phase mismatch varies with tissue relaxation parameters, as shown in Figure 5. Note that the cerebrospinal fluid (CSF) signal of spoiled STFR drops significantly faster than for other tissues, and faster than the unspoiled STFR CSF signal.

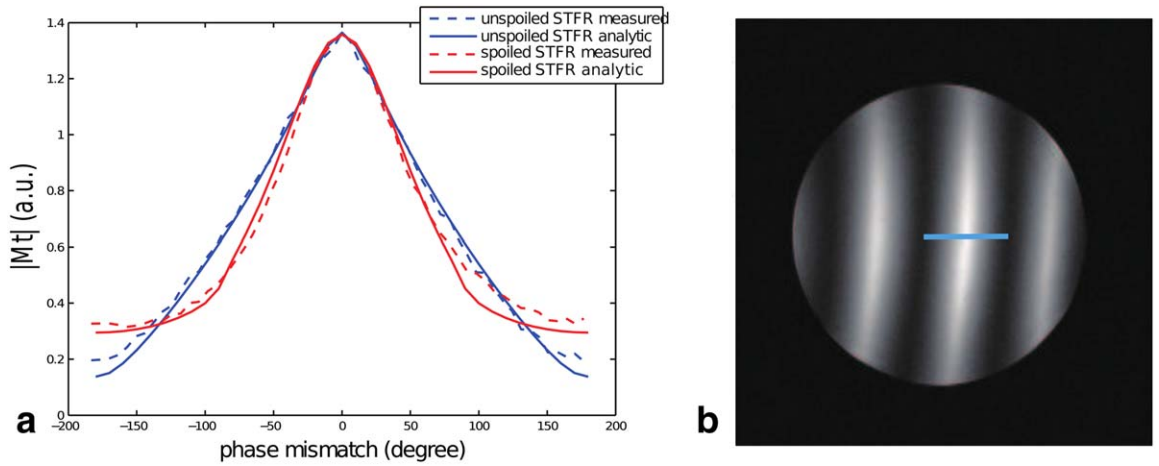

FIG. 4. **a**: Steady-state signal for unspoiled STFR and spoiled STFR as a function of phase mismatch $\phi - \theta_f$, using the analytic result from Eq. [2] and Eqs. [1,2] in Ref. (6), respectively, ($T_1/T_2 = 510/50$ ms, $T_{free}/TR = 9/12\text{ms}, \alpha = \beta = 16^\circ$) and phantom observations. Note that the rate of signal drop due to phase mismatch is smaller for unspoiled STFR. We obtained the measured curves by applying a linear gradient shim in the *x* direction and imaging a gel phantom [shown in (**b**)] with nontailored (sinc) pulses. We stress that the image in (b) was obtained for the sole purpose of obtaining the curve in (a), and is not representative of a typical STFR image acquisition. In particular, the goal in STFR is generally to design a tailored tip-up pulse that minimizes the phase mismatch and hence maximizes the signal within a target ROI. [Color figure can be viewed in the online issue, which is available at wileyonlinelibrary.com.]

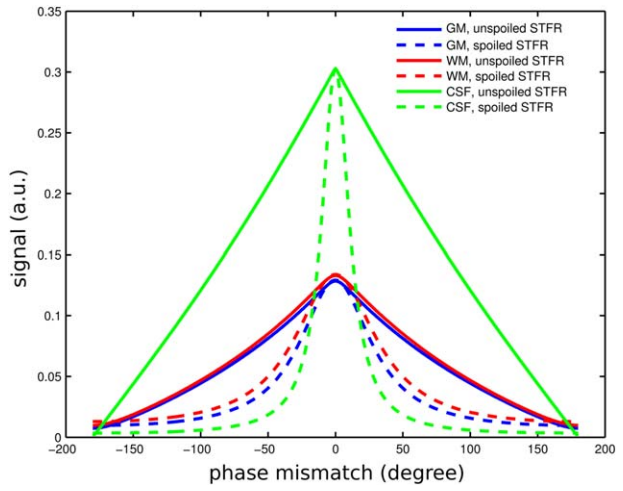

FIG. 5. Steady-state signal for unspoiled STFR and spoiled STFR as a function of phase mismatch $\phi - \theta_f$ for different tissues: gray matter (GM), white matter (WM), and cerebrospinal fluid (CSF). These calculations assumed $T_1/T_2 = 4000/2000$, 1470/71, and 1110/56ms for CSF, GM, and WM, respectively (12), and $T_{\text{free}}/\text{TR} = 7/10\text{ms}, \alpha = \beta = 20°$. The spoiled STFR sequence is more sensitive to phase mismatch compared to unspoiled STFR for all three tissue types, and especially for CSF. [Color figure can be viewed in the online issue, which is available at wileyonlinelibrary.com.]

RF Pulse Design

The key to successful STFR imaging is to design accurate tailored tip-up pulses that bring the magnetization close to the longitudinal axis. Here, we consider 3D imaging using unspoiled STFR, and we restrict our designs to nonslice-selective 3D tailored pulses. (Although we could in principle use slice- or slab-selective 3D pulses, such pulses would most likely be prohibitively long.) We propose two different approaches to RF pulse design in STFR: "Separate" and "Joint".

In our first approach, we design the tip-down and tip-up pulses independently, as follows: First, we tailor the tip-down pulse $\alpha(\mathbf{r})$ to a uniform magnitude excitation pattern with phase $-\theta_f(\mathbf{r})/2$, i.e., half the expected free precession angle. We then design an "intermediate" tip-down pulse $\beta_{\text{int}}(\mathbf{r})$ tailored to the expected spin phase at the end of T_{free}, i.e., $\angle\alpha(\mathbf{r}) + \theta_f(\mathbf{r})$. Finally, we obtain the tip-up pulse $\beta(\mathbf{r})$ by "rewinding" the intermediate pulse $\beta_{\text{int}}(\mathbf{r})$ as in (6), i.e., by time-reversing and negating $\beta_{\text{int}}(\mathbf{r})$. The advantage of this approach is that it is relatively easy to implement, e.g., using existing methods for small-tip RF pulse design.

The second approach to RF pulse design in STFR is based on the observation that the phase of tip-down pulse $\angle\alpha(\mathbf{r})$ does not in general need to be constrained to a particular pattern, as long as it varies reasonably smoothly across the ROI. In fact, the only requirement that should be imposed on the tip-down pulse is that the magnitude $|\alpha(\mathbf{r})|$ should be as uniform as possible to avoid image shading. Using the small-tip (Fourier) approximation in which the transverse component of the excitation pattern is expressed as a linear transformation of the time-varying RF waveform (13), this requirement can be stated as

$$\mathbf{sin\alpha} = |A_1\mathbf{b_1}| \qquad [3]$$

where $\mathbf{b}_1$ is a discretization of the time-varying tip-down RF waveform $b_1(t)$, and $\boldsymbol{\alpha}$ is the desired (uniform) flip angle. A_1 is a system matrix with elements $a_{ij} = \imath\gamma M_0 e^{-\imath k(t_j) r_i - \imath\Delta\omega(r_i)(t_j - T)}$, where $k(t)$ is the excitation k-space trajectory determined by the gradient waveforms for tip-down part and T is the duration of tip-down pulse. Similarly, we require that the magnitude of the magnetization after the tip-up pulse be as small as possible:

$$|A_2\mathbf{b_1} + A_3\mathbf{b_2}| = 0 \qquad [4]$$

where A_2 and A_3 are blocks of $\tilde{A} = [A_2 \;\; A_3]$ with elements $\tilde{a}_{ij} = \imath\gamma M_0 e^{-\imath\tilde{k}(t_j) r_i - \imath\Delta\omega(r_i)(t_j - \tilde{T})}$, where $\tilde{T}$ and $\tilde{k}(t)$ are the duration and excitation k-space trajectory determined by the gradient waveforms for the whole combined pulse, i.e., including tip-down excitation, free precession, and tip-up recovery.

We propose to solve Eqs. [3] and [4] jointly using the following magnitude least-squares formulation:

$$\begin{bmatrix} \hat{\mathrm{b}}_1 \\ \hat{\mathrm{b}}_2 \end{bmatrix} = \underset{\mathbf{b_1},\mathbf{b_2}}{\operatorname{argmin}} \left\{ \left\| \begin{bmatrix} \mathbf{sin}(\alpha) \\ \mathbf{0} \end{bmatrix} - \begin{bmatrix} A_1 & 0 \\ A_2 & A_3 \end{bmatrix} \begin{bmatrix} \mathbf{b_1} \\ \mathbf{b_2} \end{bmatrix} \right\|_2^2 + \mu \left\| \mathbf{b_1} \right\|_2^2 + \mu \left\| \mathbf{b_2} \right\|_2^2 \right\}, \qquad [5]$$

where μ is a Tikhonov regularization parameter that constrains the total RF energy (14). Although the joint formulation in Eq. [5] is more computationally intensive than the Separate design, it may allow for improved tip-up accuracy for a given RF pulse duration as we are removing the constraints on spin phase.

METHODS

We performed imaging experiments on a GE (General Electric Company) 3T scanner equipped with a quadrature transmit/receive head coil. Table 1 lists the various image acquisitions. The phantom was a GE resolution phantom, and the human subject was a healthy volunteer.

Table 2 lists the sequence timing for STFR and bSSFP. All image acquisitions used 256 × 256 × 65 matrix size, 24 × 24 × 24 cm field of view (FOV), and 62.5 KHz receive bandwidth. We used a FOV along z that was large enough to eliminate aliasing from untargeted slices, which in practice could be avoided by, e.g., aligning the frequency encoding direction with the z direction (15). The bSSFP acquisitions used twice the flip angle as the STFR acquisitions, as our equation and simulations predict that bSSFP will give the same (on-resonance) signal level with twice the flip angle of the STFR sequence. For the STFR acquisitions, we tailored the RF pulses to a 3D ROI consisting of a 3-cm axial slab. For this purpose, we obtained a $B0$ map of the ROI using spoiled gradient echo (SPGR) with echo times 3 and 5 ms. For the tailored pulses (both tip-down and tip-up), we used the spiral nonselective excitation k-space trajectory proposed in (15). For the Separate design, we calculated the B1 waveforms using the small-tip iterative RF pulse design

Table 1
Summary of Phantom and Human Imaging Experiments

Object	Sequence	RF pulse	Flip angle	TR (ms)
Phantom	Spoiled gradient echo (SPGR, FLASH)	Sinc	20	10
Phantom	SSFP-FID (GRASS, FISP)	Sinc	20	10
Phantom	bSSFP (FIESTA, TrueFISP)	Sinc	40	7.6
Phantom	Spoiled STFR	Tailored (Separate)	20	10
Phantom	Unspoiled STFR	Tailored (Separate)	20	10
Phantom	Unspoiled STFR	Tailored (Joint)	20	10
Brain	bSSFP (FIESTA, TrueFISP)	Sinc	40	7.6
Brain	Spoiled STFR	Tailored (Separate)	20	10
Brain	Unspoiled STFR	Tailored (Separate)	20	10
Brain	Unspoiled STFR	Tailored (Joint)	20	10

method in (14). For the Joint design, we obtained the B1 waveforms by performing the magnitude least-square minimization in Eq. [5] using the method in (16). Both designs were implemented with the MATLAB image reconstruction toolbox from University of Michigan (http://www.eecs.umich.edu/~fessler). An example of the resulting B1 waveforms and spiral nonselective gradients are shown in Figure 1b.

RESULTS

Phantom Observations

Figure 6 shows steady-state images of one of the target slices in the resolution phantom acquired with several different sequences, displayed using the same gray scale. For each image, the mean signal and standard deviation within the object are indicated. We observe a characteristic banding artifact in the bSSFP image, which is largely removed in the Joint unspoiled STFR acquisition. However, some nonuniformity remains in the Joint unspoiled STFR image, due to the limited ability to correct for B0 inhomogeneity over the ROI with the short (1.7 ms) RF pulses used here. Furthermore, STFR and (on-resonance) bSSFP have similar signal levels, about twice as high as steady-state free precession-FID like (SSFP-FID) and significantly higher than SPGR, in agreement with theory. We also observe that unspoiled STFR produces more uniform images than spoiled STFR, as predicted. Finally, we note that Joint design produces a modest improvement in mean signal level (1.41) compared to Separate design (1.36). Based on this comparison experiment, we think the Joint unspoiled version is more suitable than other STFR sequences for 3D imaging.

In vivo Observations

Figure 7a shows steady-state images from the same slice obtained with bSSFP (180° RF phase cycling) and STFR. Similar to Figure 6, we observe a banding artifact in the bSSFP image (arrow) that is not present in the unspoiled STFR image. Apart from the banding region, unspoiled STFR and bSSFP have similar signal levels and exhibit similar tissue contrast (e.g., bright CSF), as desired. The unspoiled STFR images still have signal loss in some regions due to phase mismatch (see Figure 7b), but it is much more uniform than spoiled STFR, as predicted. We observe significant CSF signal loss in the spoiled STFR image in some regions (see, e.g., oval), which can be explained by comparing the phase mismatch in that region and the phase mismatch sensitivity plot (Fig. 5). The Joint design slightly improves image quality compared to the Separate design, i.e., Joint unspoiled STFR produces a more uniform image with better contrast, and we think this improvement is due to the decrease of phase mismatch using the Joint design. Finally, the high through-plane vessel signal in bSSFP is suppressed in the STFR images (see, e.g., box), which is generally desirable.

Figure 8a compares Joint unspoiled STFR and bSSFP in five adjacent slices spanning a 4-cm FOV along z (S/I), and highlights the ability of the proposed sequence to image a 3D ROI. The top two rows show bSSFP images obtained with 0° and 180° RF phase cycling, whereas the bottom row shows the Joint unspoiled STFR images. Both bSSFP acquisitions suffer from banding artifacts. The Joint unspoiled STFR sequence achieves similar signal level and tissue contrast as bSSFP over most of the FOV, although we observe some nonuniformity (image shading) due to large phase mismatch in some region, (see Figure 8b). Note that the observation FOV (4 cm) along z is larger than the target FOV (3 cm) of the tailored pulse; however, we can still get reasonably good images in the whole observation FOV because the excitation pattern and free precession accumulated phase pattern are all relatively smooth here.

Table 2
Sequence Timing

Sequence	Tip-down (ms)	Readout (ms)	Tip-up (ms)	Gradient crusher (ms)
STFR	1.7	4.9	1.7	1.2
bSSFP	1.2	4.9	n/a	n/a

DISCUSSION

Our theory predicts that STFR has similar SNR as bSSFP (see Figure 3), which agrees with our measured results (44.2/45.3 and 31.6/32.4 dB for bSSFP/STFR in phantom and gray matter ROIs, respectively). Therefore, the SNR efficiency (defined as $\mathrm{SNR}/\sqrt{\text{total scan time}}$) of STFR will be lower than on-resonance bSSFP, as its TR is necessarily longer than the corresponding bSSFP sequence. Compared to multiple phase-cycled bSSFP acquisitions, whether STFR is more SNR efficient or not depends on

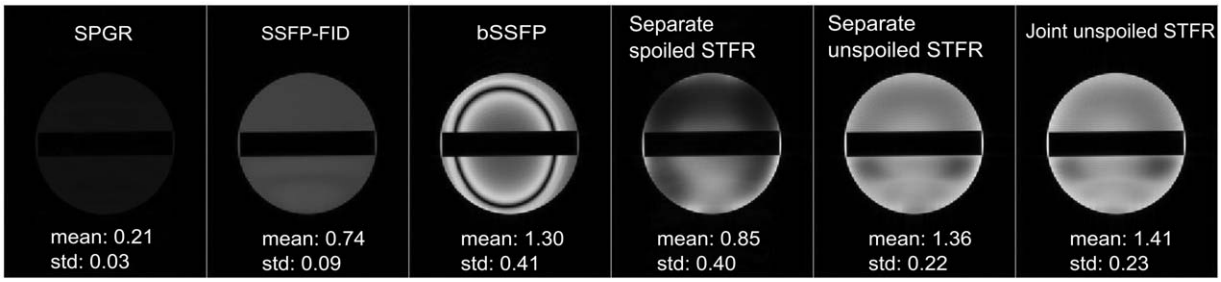

FIG. 6. Steady-state imaging, phantom results. Images are shown on the same gray scale. For each image, the mean signal and standard deviation within the object are indicated. Unspoiled STFR with the proposed "Joint" RF pulse design (right) produces signal levels that are comparable to on-resonance bSSFP, and has improved uniformity compared to bSSFP and spoiled STFR. Unspoiled STFR with the simpler "Separate" RF pulse design approach (second from right) shows improved signal and uniformity compared to spoiled STFR, but slightly lower overall signal compared to the Joint design. Conventional SPGR and SSFP-FID images are included for reference.

the actual timing of the specific sequences and the method used to combine the phase-cycled images. In our experiments, we use TR = 7.6 and 10 ms for bSSFP and STFR, respectively. The TR of bSSFP is not optimized in our experiment and can be as low as 6.8 ms given our scanner control code and the same readout time (4.9 ms) as STFR. Assuming TR = 6.8 ms for bSSFP and TR = 10 ms for STFR, the total scan time of STFR is 1/1.36 of two phase-cycled bSSFP and 1/2.04 of three phase-cycled bSSFP. Conversely, the SNR increases by combining the phase-cycled bSSFP images, and the amount of increase depends on the tissue parameters, noise level, and the combination method (8). For simplicity, if we assume maximum intensity combination, STFR as implemented in our experiments would have similar SNR efficiency as two phase-cycled bSSFP, and better SNR efficiency than three phase-cycled bSSFP. It is, therefore, possible that in applications where image SNR is critical, bSSFP with two phase-cycles may be preferred over STFR. We note, however, that multiple acquisitions may not be preferred in some applications. For example, in bSSFP functional magnetic resonance imaging, repeating

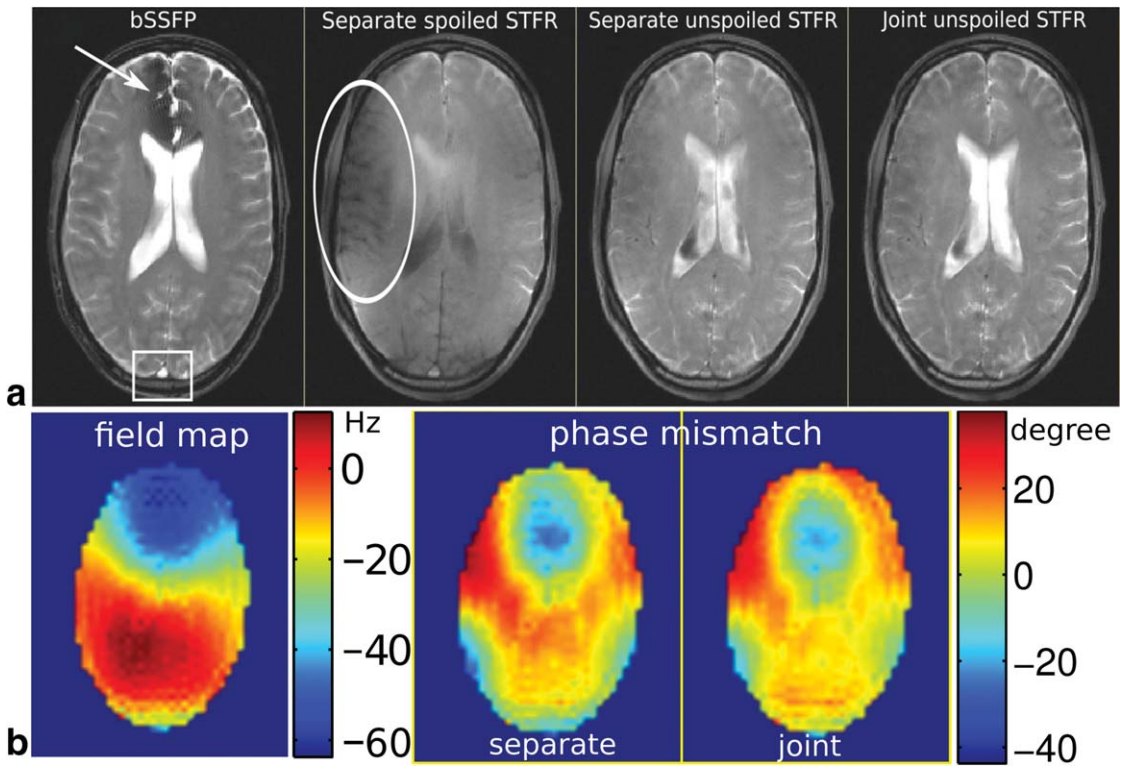

FIG. 7. **a**: Comparison of bSSFP (left) with three different STFR acquisitions, in the same slice. **b**: Field map and phase mismatch maps using Separate and Joint design. Banding artifacts in the anterior part (arrow) of the bSSFP image are largely absent in the unspoiled STFR images. Spoiled STFR is less uniform than unspoiled STFR as predicted, and the signal drops more in the region with high phase mismatch. Note that the CSF in the oval region in the spoiled STFR image drops significantly more than the nearby tissue signal and the unspoiled STFR CSF signal, which agrees with the phase mismatch map and sensitivity to phase mismatch plot in Figure 5. The Joint design has slightly smaller phase mismatch, which leads to improved signal uniformity and tissue contrast compared to the Separate design. Also, note that the high through-plane vessel signal in the bSSFP image is suppressed in the STFR images (see, e.g., box).

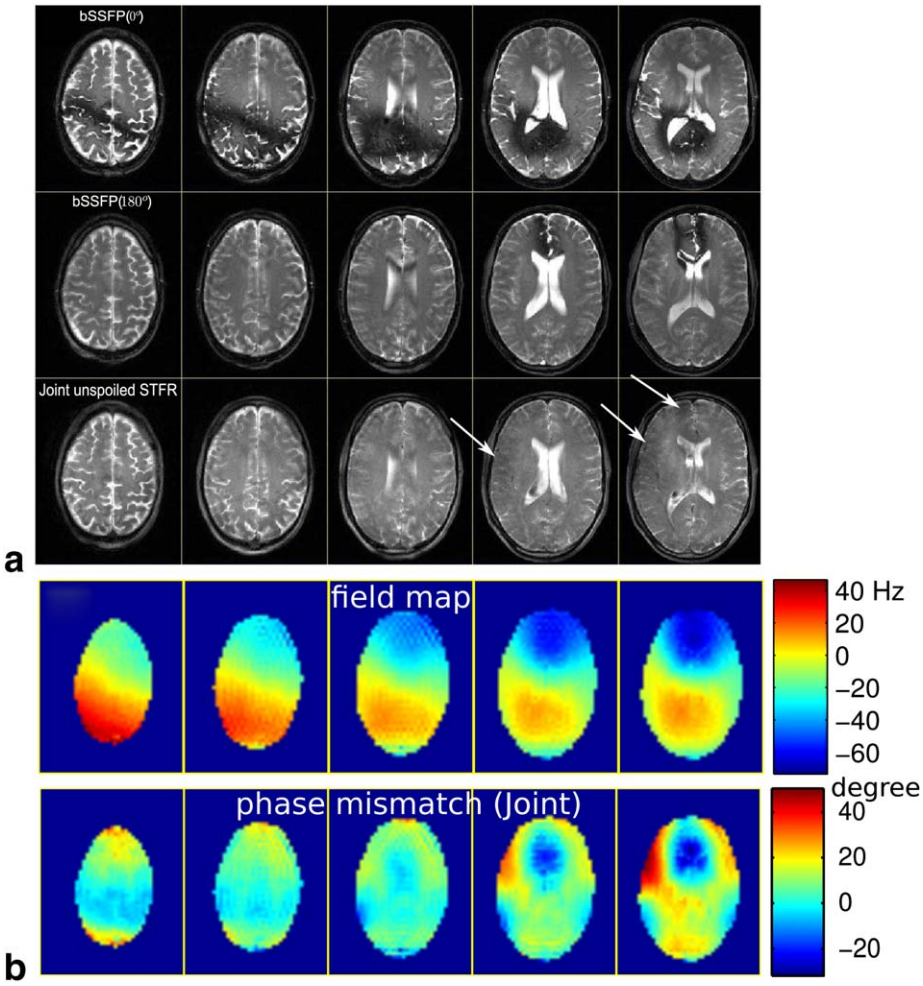

FIG. 8. **a**: Proof-of-principle demonstration of 3D unspoiled STFR imaging, using Joint 3D tailored RF pulses. Images are shown for Joint unspoiled STFR, and bSSFP with different phase cycling schemes, in five adjacent axial slices spanning 4 cm: (top) 0° phase cycled bSSFP; (middle) 180° phase cycled bSSFP; (bottom) Joint unspoiled STFR. Both bSSFP acquisitions suffer from banding artifacts, which are reduced with the 3D Joint unspoiled STFR sequence. **b**: Field map and phase mismatch maps. The STFR signal drops more in the region with high phase mismatch [See, e.g., arrows in (a)]. [Color figure can be viewed in the online issue, which is available at wileyonlinelibrary.com.]

runs of a paradigm produces confounding effects from cognitive habituation to stimuli and is not ideal (17,18). Alternating bSSFP that interleaves two phase-cycled bSSFP imaging can potentially solve this problem (19), but it needs catalyzation pulses every time the phase-cycling is changed, which reduces its SNR efficiency.

Here, we have shown that STFR and bSSFP image contrast is similar with respect to T_1 and T_2 sensitivity, however, we have performed preliminary work that indicates that these sequences have different sensitivity to diffusion and intravoxel B0 homogeneity (20). In bSSFP, because of the relative flat magnitude and phase frequency response curve in the passband, all the spins within a voxel typically have similar magnitude and phase, therefore, there is almost no T_2^* contrast. In STFR, because of the low spatial resolution of the tailored pulse, the spins within one voxel may experience different phase mismatch due to intravoxel B0 field variation leading to a T_2^*-like contrast. This property of STFR can be used to detect blood-oxygen-level-dependent signal in functional imaging, which is reported in (20), and which will be investigated in detail in future work.

We have proposed a joint RF pulse design method for STFR, which produced a modest improvement over the Separate design. We expect that our Joint algorithm can be improved in at least two ways. First, as the Joint approach formulates a nonconvex magnitude least squares problem, it is possible that our solver gets "stuck" in a local minimum. Specifically, at each iteration, our algorithm solves a least squares problem $\text{argmin}_{\mathbf{b}} ||A\mathbf{b} - \mathbf{d}||$ whereby the phase of the target excitation pattern $\mathbf{d}$ is updated. We attempted several different initializations to the phase pattern of $\mathbf{d}$ including all zero and random phase, and achieved similar results, suggesting we may have obtained a global minimum in our experiments. However, this is not a rigorous conclusion, and it is possible that alternative solvers may improve the RF design. Second, in our Joint design formulation, we used the small tip angle approximation but we enforced the spins to be tipped down in the middle of the combined pulse. Although we are working in the small tip regime ($\leq 20^\circ$), this forced tip-down in the middle may still make the small tip angle approximation method less accurate. It is possible that our Joint design can be improved by borrowing ideas from large-tip-angle pulse design, e.g., the additive angle method (21) or designs based on perturbation analysis of the Bloch equation (22).

In addition to improving the RF pulse design algorithm, other complementary methods can be used to improve STFR imaging performance. One straightforward approach is to reduce data acquisition time and hence

T_{free}, which reduces the spatial inhomogeneity of the target phase pattern $\theta_f(\mathbf{r})$. This can be done by, e.g., using fast non-Cartesian readout trajectories. This approach may reduce the SNR but the SNR efficiency may not decrease much because the tailored pulse length may be shorter. In addition, high-order gradient shim systems can be used to reduce B0 inhomogeneity, which also makes $\theta_f(\mathbf{r})$ vary more smoothly across the ROI. This approach would benefit bSSFP as well, but shimming itself may not be sufficient to remove all the banding in bSSFP. Alternatively, parallel RF transmission should allow for improved RF pulse accuracy for a given pulse duration. Parallel excitation has been an active research area in recent years, including by our group (23), and commercial support for such systems is emerging.

A drawback of the proposed nonslice-selective imaging approach is that signal from outside the ROI may alias into the FOV. Although slab selective 3D tailored pulses could in principle be used, such pulses may be prohibitively long (24). One potential solution to this problem is to use Cartesian readout with frequency encoding in the S/I direction, i.e., using the data acquisition filter to remove signal from outside the FOV, but this approach may require longer scan time since the A/P and R/L directions must be fully phase encoded, and these directions typically have larger matrix size. Another potential solution is to use surface coils near the ROI such that signal contribution from outside the ROI is minimized.

CONCLUSIONS

We have developed a new steady-state sequence, unspoiled STFR, and demonstrated using analytic modeling and experiments that this sequence produces bSSFP-like signal and tissue contrast but with reduced banding artifacts. Our analysis shows that the proposed sequence is less sensitive to RF pulse inaccuracies than its spoiled counterpart. We have also proposed a novel Joint RF pulse design approach that formulates the RF design problem in STFR as a magnitude least-squares minimization problem, modestly improving image quality. With this approach, we have demonstrated that brain imaging over a 3–4-cm thick 3D ROI is possible using a standard quadrature transmit/receive head coil and short tailored 3D RF pulses of 1.7 ms duration. We expect that future improvements in high-order shimming or parallel transmit systems will allow expanded 3D ROIs to be imaged with the proposed approach.

APPENDIX

Define the magnetization vector as $\mathbf{M} = (M_x, M_y, M_z)^T$. Referring to Figure 1, we model each spin path segment as follows:

1. $\mathbf{M}_1$ to $\mathbf{M}_2$: Free precession and T_1, T_2 relaxation.

Define $\Delta\omega$ as the local off-resonance frequency, and T_{free} as the free precession time. The free precession phase is then $\theta_f = \Delta\omega T_{\text{free}}$. The Bloch equation in matrix form for this rotation is: $\mathbf{M}_2 = \mathbf{P}\mathbf{C}_f\mathbf{M}_1 + \mathbf{D}_f$where

$$\mathbf{C}_f = \begin{bmatrix} e^{-\frac{T_{\text{free}}}{T_2}} & 0 & 0 \\ 0 & e^{-\frac{T_{\text{free}}}{T_2}} & 0 \\ 0 & 0 & e^{-\frac{T_{\text{free}}}{T_1}} \end{bmatrix}, \mathbf{D}_f = (\mathbf{I} - \mathbf{C}_f)\begin{bmatrix} 0 \\ 0 \\ M_0 \end{bmatrix}, \mathbf{P} = \begin{bmatrix} \cos\theta_f & \sin\theta_f & 0 \\ -\sin\theta_f & \cos\theta_f & 0 \\ 0 & 0 & 1 \end{bmatrix}$$

2. $\mathbf{M}_2$ to $\mathbf{M}_3$: "Tip-up" RF pulse with phase ϕ and flip angle β.

$$\mathbf{M}_3 = \mathbf{R}_u\mathbf{M}_2$$

where

$$\mathbf{R}_u = \begin{bmatrix} \cos\phi & \sin\phi & 0 \\ -\sin\phi & \cos\phi & 0 \\ 0 & 0 & 1 \end{bmatrix}\begin{bmatrix} 1 & 0 & 0 \\ 0 & \cos\beta & -\sin\beta \\ 0 & \sin\beta & \cos\beta \end{bmatrix}\begin{bmatrix} \cos\phi & -\sin\phi & 0 \\ \sin\phi & \cos\phi & 0 \\ 0 & 0 & 1 \end{bmatrix}$$

3. $\mathbf{M}_3$ to $\mathbf{M}_4$: Unbalanced gradient g rotates $\mathbf{M}$ about z axis by θ_g. Also include T_1, T_2 relaxation.

$$\mathbf{M}_4 = \mathbf{G}\mathbf{C}_g\mathbf{M}_3 + \mathbf{D}_g$$

where

$$\mathbf{G} = \begin{bmatrix} \cos\theta_g & \sin\theta_g & 0 \\ -\sin\theta_g & \cos\theta_g & 0 \\ 0 & 0 & 1 \end{bmatrix},$$

$$\mathbf{C}_g = \begin{bmatrix} e^{-\frac{T_g}{T_2}} & 0 & 0 \\ 0 & e^{-\frac{T_g}{T_2}} & 0 \\ 0 & 0 & e^{-\frac{T_g}{T_1}} \end{bmatrix}, \mathbf{D}_g = (\mathbf{I} - \mathbf{C}_g)\begin{bmatrix} 0 \\ 0 \\ M_0 \end{bmatrix},$$

4. $\mathbf{M}_4$ to $\mathbf{M}_1$: The tip-down pulse rotates $\mathbf{M}$ about the x axis by α.

$$\mathbf{M}_1 = \mathbf{R}_d\mathbf{M}_4$$

where

$$\mathbf{R}_d = \begin{bmatrix} 1 & 0 & 0 \\ 0 & \cos\alpha & \sin\alpha \\ 0 & -\sin\alpha & \cos\alpha \end{bmatrix}$$

Combining these steps and requiring that the magnetization reaches a steady-state, we obtain:

$$\mathbf{M}_1 = \mathbf{R}_d\left(\mathbf{G}\mathbf{C}_g\left(\mathbf{R}_u\left(\mathbf{P}\mathbf{C}_f\mathbf{M}_1 + \mathbf{D}_f\right)\right) + \mathbf{D}_g\right)$$
$$\Rightarrow \mathbf{M}_1 = \left(\mathbf{I} - \mathbf{R}_d\mathbf{G}\mathbf{C}_g\mathbf{R}_u\mathbf{P}\mathbf{C}_f\right)^{-1}\left(\mathbf{R}_d\mathbf{G}\mathbf{C}_g\mathbf{R}_u\mathbf{D}_f + \mathbf{R}_d\mathbf{D}_g\right)$$

We obtain an expression for the transverse part of **M**, i.e., Eq. [1], by simplifying the above expression using symbolic math software (MATHEMATICA 8, Wolfram, Champaign, IL). The MATHEMATICA code is available on our website (http://www.umich.edu/~sunhao).

ACKNOWLEDGMENTS

The authors thank Dr. Shaihan Malik for providing MATLAB scripts for generating the SPINS excitation k-space trajectory.

REFERENCES

1. Scheffler K, Lehnhardt S. Principles and applications of balanced SSFP techniques. Eur Radiol 2003;13:2409–2418.
2. Overall WR, Nishimura DG, Hu BS. Steady-state sequence synthesis and its application to efficient fat-suppressed imaging. Magn Reson Med 2003;50:550–559.
3. Çukur T, Lustig M, Nishimura DG. Improving non-contrast-enhanced steady-state free precession angiography with compressed sensing. Magn Reson Med 2009;61:1122–1131.
4. Nayak KS, Lee HL, Hargreaves BA, Hu BS. Wideband SSFP: alternating repetition time balanced steady state free precession with increased band spacing. Magn Reson Med 2007;58:931–938.
5. Leupold J, Hennig J, Scheffler K. Alternating repetition time balanced steady state free precession. Magn Reson Med 2006;55:557–565.
6. Nielsen JF, Yoon D, Noll DC. Small-tip fast recovery imaging using non-slice-selective tailored tip-up pulses and radiofrequency-spoiling. Magn Reson Med 2013;69:657–666.
7. Heilman JA, Derakhshan JJ, Riffe MJ, Gudino N, Tkach J, Flask CA, Duerk JL, Griswold MA. B0 and B1 correction using the inherent degrees of freedom of a multi-channel transmit array. In Proceedings of the 17th Annual Meeting of ISMRM, Honolulu, Hawaii, USA, 2009. p. 251.
8. Bangerter NK, Hargreaves BA, Vasanawala SS, Pauly JM, Gold GE, Nishimura DG. Analysis of multiple-acquisition SSFP. Magn Reson Med 2004;51:1038–1047.
9. Bieri O, Scheffler K. SSFP signal with finite RF pulses. Magn Reson Med 2009;62:1232–1241.
10. Bieri O, Scheffler K. Extended chimera SSFP. In Proceedings of the 18th Annual Meeting of ISMRM, Stockholm, Sweden, 2010. p. 76.
11. Miller KL, Jezzard P. Modeling SSFP functional MRI contrast in the brain. Magn Reson Med 2008;60:661–673.
12. Stanisz G, Odrobina E, Pun J, Escaravage M, Graham S, Bronskill M, Henkelman R. T_1, T_2 relaxation and magnetization transfer in tissue at 3T. Magn Reson Med 2005;54:507–512.
13. Pauly J, Nishimura D, Macovski A. A k-space analysis of small-tip-angle excitation. J Magn Reson 1989;81:43–56.
14. Yip C, Fessler JA, Noll DC. Iterative RF pulse design for multidimensional, small-tip-angle selective excitation. Magn Reson Med 2005;54:908–917.
15. Malik SJ, Keihaninejad S, Hammers A, Hajnal JV. Tailored excitation in 3D with spiral nonselective (SPINS) RF pulses. Magn Reson Med 2012;67:1303–1315.
16. Setsompop K, Wald LL, Alagappan V, Gagoski BA, Adalsteinsson E. Magnitude least squares optimization for parallel radio frequency excitation design demonstrated at 7 Tesla with eight channels. Magn Reson Med 2008;59:908–915.
17. Lee JH, Dumoulin SO, Saritas EU, Glover GH, Wandell BA, Nishimura DG, Pauly JM. Full-brain coverage and high-resolution imaging capabilities of passband b-SSFP fMRI at 3T. Magn Reson Med 2008;59:1099–1110.
18. Miller KL, Hargreaves BA, Lee J, Ress D, deCharms RC, Pauly JM. Functional brain imaging using a blood oxygenation sensitive steady state. Magn Reson Med 2003;50:675–683.
19. Patterson S, Mazerolle E, Beyea S, Bowen C. Whole-brain artifact-suppressed SSFP fMRI in a single paradigm run: alternating SSFP. In Proceedings of the 20th Annual Meeting of ISMRM, Melbourne, Australia, 2012. p. 2309.
20. Nielsen JF, Sun H, Fessler JA, Noll DC. Steady-state functional MRI using small-tip fast recovery (STFR) imaging. In Proceedings of the 21st Annual Meeting of ISMRM, Salt Lake City, Utah, USA, 2013. p. 3333.
21. Grissom WA, Yip CY, Wright SM, Fessler JA, Noll DC. Additive angle method for fast large-tipangle rf pulse design in parallel excitation. Magn Reson Med 2008;59:779–787.
22. Zheng H, Zhao T, Qian Y, Ibrahim TS, Boada FE. Improved large tip angle parallel transmission pulse design through a perturbation analysis of the bloch equation. Magn Reson Med 2011;66:687–696.
23. Hollingsworth N, Moody K, Nielsen JF, Noll D, McDougall M, Wright S. An eight channel transmit system for transmit SENSE at 3T. In Proceedings of the IEEE International Symposium on Biomedical Imaging, Chicago, Illinois, USA, 2011. pp 0775–0778.
24. Yip C, Fessler JA, Noll DC. Advanced three-dimensional tailored RF pulse for signal recovery in T_2^*-weighted functional magnetic resonance imaging. Magn Reson Med 2006;56:1050–1059.